HHS Public Access

Author manuscript

Nature. Author manuscript; available in PMC 2011 February 01.

Published in final edited form as:

Nature. 2010 August 12; 466(7308): 874–878. doi:10.1038/nature09249.

Wnt11 patterns a myocardial electrical gradient via regulation of the L-type Ca^{2+} channel

Daniela Panáková[1,*], **Andreas A. Werdich**[1,*], and **Calum A. MacRae**[1]

[1]Brigham and Women's Hospital/Harvard Medical School, Cardiovascular Division, 75 Francis Street, Thorn 11, Boston, MA 02115

Abstract

Electrical gradients are critical for many biological processes, including the normal function of excitable tissues, left-right patterning, organogenesis, and wound healing1–4. The fundamental mechanisms that regulate the establishment and maintenance of such electrical polarities are poorly understood. Using high-speed optical mapping of transmembrane potentials and calcium concentrations in the zebrafish heart, we have identified a gradient of electrical coupling across the developing ventricular myocardium. We excluded a role for cellular excitability, connexin localization, tissue geometry and mechanical inputs, but in contrast we were able to demonstrate that non-canonical Wnt11 signals are required for the genesis of this myocardial electrical gradient. Importantly, though the traditional planar cell polarity pathway is not involved, we obtained evidence that Wnt11 acts to set up this gradient of electrical coupling through effects on transmembrane Ca^{2+} conductance mediated via the L-type calcium channel. These data reveal a previously unrecognized role for Wnt/Ca^{2+} signaling in establishing an electrical gradient in the plane of developing cardiac epithelium through modulation of ion channel function. The regulation of cellular coupling through such mechanisms may be a general property of non-canonical Wnt signals.

Zebrafish cardiomyocytes begin to spontaneously depolarize in the bilateral cardiac primordia before they assemble into the linear heart tube and by 24 hours post fertilization (hpf), synchronous contractions start. Over the next 24 hours the heart loops and atrium and ventricle form. During morphogenesis, intercellular coupling between differentiating cardiomyocytes is established and refined. Studies of higher vertebrates suggest that transmural and apex-to-base electrical gradients, which emerge during development, are crucial for the electrical stability and mechanical efficiency of the adult heart5. Using high-speed optical mapping of transmembrane potentials we characterized electrical conduction in the embryonic zebrafish heart at cellular resolution (Methods and Supplementary Fig. 1). At 24hpf, action potentials propagate slowly and homogenously throughout the linear heart tube (Fig. 1a, c, Supplementary Movie 1). From 48hpf there is substantial acceleration of

---

Correspondence and requests for materials should be addressed to C.A.M. (camacrae@bics.bwh.harvard.edu).

*These authors contributed equally to this work.

Supplementary Information accompanies the paper at www.nature.com/nature.

impulse propagation in both chambers with the concomitant emergence of zones of slow conduction at sinoatrial, atrioventricular and ventriculo-aortic boundaries (Fig. 1b, Supplementary Movie 2), as previously revealed using lower resolution techniques6,7. We observed a gradient of impulse propagation velocities across the ventricle (Fig. 1b); outer curvature (OC) myocardium, that becomes the ventricular apex, conducts action potentials three times faster than the inner curvature (IC), the future ventricular base (Fig. 1c). This electrical gradient emerges at 48hpf and persists into larval stages (Fig. 2h). These data demonstrate functional heterogeneity across the plane of the cardiac epithelium even in the two-chambered zebrafish heart.

To address whether the OC-to-IC electrical gradient results from differences in excitability, we compared action potential upstrokes in these myocardial zones. Action potential upstrokes were monophasic and the rates of change of transmembrane potential comparable in both OC and IC cells (Fig. 1d, e). We next looked at intercellular electrical coupling, which is mainly facilitated by gap junction proteins; the connexins8. In the developing zebrafish heart, connexin 43 (Cx43) is the first major detectable connexin7. Semiquantitative immunostaining revealed that Cx43 is approximately twice as abundant in the atrium as in the ventricle, but did not result in any differences in Cx43 localization between OC and IC cells (Fig. 1f, g). While neither excitability nor differential Cx43 localization appear to explain the myocardial electrical gradient, it remains possible that changes in the localization of other connexins or connexin function play a role.

Cellular architecture is known to affect impulse propagation across the myocardium9. Recently, OC and IC cardiomyocytes in wildtype zebrafish ventricles have been reported to acquire distinct cell shapes during chamber formation, with their final shape depending on contractile function10. To assess the role of these physical factors on the electrical gradient, we measured conduction velocities in two non-contractile mutants: *silent heart*, a recessive cardiac troponin T mutant11 and *unc45b*, a recessive mutant in a chaperone required for assembly of myofibers12. We confirmed prior reports that cell architecture is disrupted in non-contractile hearts (Fig. 1h–j)10. While conduction velocities are increased in these mutants, the OC-to-IC electrical gradient was comparable to that of wildtype hearts (Fig. 2a, b, Supplementary Fig. 2a). These data show that mechanical forces regulate cell shape and modulate action potential propagation, but do not perturb patterning of electrical coupling across the myocardium.

The roles of Wnt canonical and non-canonical pathways in cardiogenesis are well documented13. Importantly, Wnt11 non-canonical signaling has been identified as a critical regulator of heart development14–17. To test whether such Wnt signals pattern electrical coupling, we focused on two non-canonical Wnts: Wnt5 and Wnt11, that are both expressed in pharyngeal arches, adjacent to the developing heart18. Using previously validated morpholinos we reduced Wnt5 and Wnt11 levels19,20 and measured ventricular conduction velocities. While loss of Wnt5 did not abolish the differential electrical coupling between OC and IC cells (Fig. 2c, e), loss of Wnt11 prevented formation of the electrical gradient and resulted in homogenous conduction velocities across the entire ventricle (Fig. 2d, f, Supplementary Movie 3). We examined expression of Wnt11 in greater detail to assess its role in the formation of the electrical gradient. In addition to previously characterized

expression domains, we detected Wnt11 RNA in the outflow tract from 48hpf onwards and in the ventricle by 72hpf where it persists at least until 120hpf (Supplementary Fig. 3). In Wnt11 morphant hearts at 72hpf, while the morpholino effect is still present, the conduction velocities between OC and IC were almost identical. However by 120hpf, the electrical gradient was restored, suggesting that Wnt11 actively patterns electrical coupling through these stages of development (Fig. 2h). Corroborating these results, we observed that the electrical gradient does not form in the Wnt11 mutant *silberblick*21 (Fig. 2g, h and Supplementary Fig. 2b–d). These data demonstrate that Wnt11 is specifically required for both the establishment and maintenance of the ventricular electrical gradient and also suggest that the remodeling of intercellular electrical coupling is a dynamic process that may last throughout development.

Wnt/β-catenin-independent signaling acts via two major downstream cascades: the planar cell polarity (PCP) pathway and Ca^{2+} signaling22. We first explored a role for the PCP pathway in patterning the electrical gradient by measuring conduction velocities in the absence of two of its essential components, Vangl2 and Prickle1a23,24. The OC-to-IC electrical gradient was maintained in both *vangl2* null mutant hearts and in Prickle1a morphant hearts, in which Prickle1a levels were reduced using a previously validated morpholino (Fig. 2i, j, Supplementary Fig. 2e, f). While OC conduction velocities were decreased in Prickle1a morphant hearts, in comparison to *vangl2* mutants, the electrical gradient was nevertheless unperturbed. We also noticed that in *vangl2* mutants as well as in Wnt11 and in Prickle1a morphants, heart morphogenesis and cellular architecture were disrupted (Supplementary Fig. 2g–i). These data support the independence of the electrical gradient from cellular architecture and suggest that PCP signaling is not responsible for its patterning.

Ca^{2+} has been identified as an important second messenger in Wnt non-canonical signaling more than a decade ago25. Subsequent studies have revealed several distinct members of the Wnt/Ca^{2+} pathway22. However, the most proximal events of Wnt/Ca^{2+} signaling remain incompletely understood. In cardiomyocytes, intracellular Ca^{2+} concentrations ($[Ca^{2+}]_i$) change substantially within milliseconds during the excitation-contraction cycle, with baseline $[Ca^{2+}]_i$ levels attained at diastole and maximum concentrations at systole (Fig. 3a). This phasic $[Ca^{2+}]_i$ transient requires the orchestrated operation of multiple ion channels and transporters; including the L-type Ca^{2+} channel (LTCC), the major transmembrane Ca^{2+} conductance channel, and SERCA, the sarcoplasmic reticulum (SR) Ca^{2+}ATP-ase, which actively transports Ca^{2+} into the SR26.

To examine the role of Ca^{2+} in regulating the electrical gradient downstream of Wnt11, we used high-speed ratiometric calcium imaging and measured $[Ca^{2+}]_i$ transients in embryonic zebrafish hearts. Diastolic $[Ca^{2+}]_i$ (Supplementary Fig. 4a) and the amplitude of the $[Ca^{2+}]_i$ transients as measured by $[Ca^{2+}]_i$(sys) - $[Ca^{2+}]_i$ (dia) were initially estimated in wildtype hearts (Fig. 3a, b, d, Supplementary Fig. 4c). Loss of Wnt11 did not perturb diastolic $[Ca^{2+}]_i$ (Supplementary Fig. 4b), but resulted in a significant increase in the amplitude of the $[Ca^{2+}]_i$ transient (Fig. 3a, c, d, Supplementary Fig. 4d) when compared to wildtype. Notably, loss of Wnt11 signaling also leads to an increase in heterogeneity of $[Ca^{2+}]_i$ transient amplitudes

across the entire ventricle (Supplementary Fig. 4d), supporting the notion that Wnt11 modulates Ca^{2+} homeostasis.

There are several possible mechanisms by which Wnt11 might regulate changes in $[Ca^{2+}]_i$. In non-excitable tissues, Wnt overexpression increases $[Ca^{2+}]_i$ transient frequency, through Ca^{2+} release from the intracellular stores (Supplementary Fig. 7)25. To isolate the effects of Wnt11 on SR Ca^{2+} stores in cardiomyocytes, we eliminated transmembrane Ca^{2+} entry through pharmacologic or genetic loss of LTCC function. Remarkably, both the LTCC antagonist nifedipine and the LTCC null mutant *cacna1c*^{m231} increased the $[Ca^{2+}]_i$ transient amplitude (Fig. 3a, d, e, Supplementary Fig. 5a)27. This effect was abolished in *cacna1c*^{m231} mutants treated with thapsigargin and caffeine (TgC), a drug combination that depletes SR Ca^{2+} stores (Fig. 3a, f,) suggesting that it is largely due to enhanced SR Ca^{2+} release. Nevertheless, both nifedipine-treated and *cacna1c*^{m231} mutant ventricles exhibited wildtype electrical gradients (Fig. 3g–i, Supplementary Fig 5b). Incubating wildtype zebrafish embryos with the LTCC agonist Bay-K 8644 increased the $[Ca^{2+}]_i$ transient amplitude as expected (Fig. 4a, b, Supplementary Fig. 5c). This increase in transmembrane Ca^{2+} influx abolished the emergence of the normal electrical gradient and reproduced the Wnt11 loss-of-function conduction phenotype (Fig. 4c, d). Similarly, by incubating wildtype hearts with TgC, we also observed an increase in the $[Ca^{2+}]_i$ transient amplitude (Fig. 4a, b, Supplementary Fig. 5d). This effect was presumed to result largely from changes in transmembrane Ca^{2+}conductance through the LTCC, as $[Ca^{2+}]_i$ transients were virtually abolished in TgC-treated *cacna1c*^{m231} hearts (Fig. 3a, f). We confirmed the loss of the OC-to-IC electrical gradient in the TgC-treated hearts (Fig. 4e, f). Thus, increasing the $[Ca^{2+}]_i$ transient amplitude through LTCC, via direct or indirect means, leads to a loss of the myocardial electrical gradient. Of note, the paradoxical reciprocal increases in Ca^{2+} transient amplitude seen with attenuation of transmembrane or SR Ca^{2+} fluxes may represent a mechanism by which Wnt signals regulate Ca^{2+} dynamics between discrete intracellular domains (see model in Supplementary Fig. 7).

These data suggest that Wnt11-mediated attenuation of transmembrane Ca^{2+} influx through the LTCC is responsible for emergence of a physiologic electrical gradient. In order to test this definitively we explored the effects of loss of Wnt11 in *cacna1c*^{m231} mutants. In this context, the gradient of electrical coupling was unaltered compared to that of the wildtype hearts (Fig 4g). Similarly, the electrical gradient was preserved in Wnt11 morphants treated with LTCC antagonist nifedipine (Fig 4h). These data demonstrate that Wnt11 acts upstream of the LTCC, down-regulating LTCC function, as the electrical gradient is established in the developing ventricle. Corroborating these findings is the absence of any effect on electrical coupling when extreme changes in SR Ca^{2+} release occurred in *cacna1c*^{m231} mutants.

In order for the electrical gradient to form, the LTCC channel must be absent or its conductance must be attenuated by a Wnt11-dependent mechanism. To determine whether gain of Wnt11 function perturbs this gradient, we over-expressed Wnt11:CFP in developing hearts under a cardiac specific promoter. The Wnt11:CFP fusion construct has been shown to be functional, rescuing the *silberblick* mutant phenotype28,29. Indeed, over-expression of Wnt11:CFP in only a few cardiomyocytes resulted in a robust non cell-autonomous phenotype that resembled Wnt11 loss-of-function, including impaired heart morphogenesis

(Supplementary Fig. 5e–h). Basal Wnt signaling is thought to be maintained within a homeostatic range30, thus opposing effects on Wnt activity could result in similar outcomes. While the strength of the Wnt11 over-expression phenotype was dose-dependent, the electrical gradient remained unperturbed across different doses (Fig. 4i, j, Supplementary Fig. 5i). These data suggest that threshold amounts rather than specific Wnt11 levels are required to attenuate the LTCC function and establish the myocardial electrical gradient.

To explore potential mechanisms through which Wnt11/LTCC signaling might remodel intercellular coupling, we assessed the effect of loss of Wnt11 on Cx43. While the levels and localization of Cx43 were comparable in the wildtype and in the *cacna1c*^{m231} mutant hearts, loss of Wnt11 lead to marked upregulation of Cx43 (Fig. 1f, 4k, Supplementary Fig. 6a–i). To determine whether this increase was Wnt11/LTCC dependent, we probed Cx43 in *cacna1c*^{m231} mutants with reduced Wnt11 and found that the Cx43 levels were comparable to those of the wildtype (Fig. 4l, Supplementary Fig. 6j–l). While regional differences in Cx43 do not explain the electrical gradient formation, these data suggest that Wnt11/LTCC signaling effects on membrane proteins may modulate connexin function or directly affect intercellular conductance (Supplementary Fig. 7).

Taken together, our data define an intrinsic electrical gradient in the developing cardiac epithelium that does not depend on specialized conduction tissue, but is sufficient to effect early activation of the cardiac apex even in a two-chambered heart. The patterning of this gradient requires Wnt11-mediated attenuation of LTCC conductance, and represents a novel effector limb in Wnt/Ca^{2+} signaling. Furthermore, these data demonstrate that Wnt11 regulates the integration of intracellular and extracellular Ca^{2+}, while also tuning dynamic relationships between subcellular Ca^{2+} domains. The refinement of electrical coupling by Wnt signals may be an important factor not only in cardiogenesis, but also in the establishment and maintenance of other epithelia in development, health and disease.

Methods Summary

Fluorescence measurements

Hearts, isolated from wildtype zebrafish embryos (24hpf to 72hpf) were stained with the transmembrane potential-sensitive dye di-8-ANEPPS (Invitrogen) or the calcium-sensitive ratiometric dye Fura-2, AM (Invitrogen) for the measurements of action potentials and calcium transients, respectively. Fluorescence intensities were recorded with a high-speed CCD camera (Redshirt Imaging).

Propagation velocity calculation

Propagation velocities of depolarizing waves were estimated as previously described, with some modifications (see full description in the online methods).

Immunostaining and image analysis

Hearts, isolated from 72hpf zebrafish embryos were fixed in Prefer fixative (Anatech Ltd.) and stained with primary antibodies: rabbit anti-connexin43 (Sigma) 1:50, mouse anti-β-catenin (BD Biosciences) 1:200, mouse anti-zn8 (DSHB) 1:50; secondary antibodies:

donkey anti-rabbit or mouse Alexa-Fluor-488 or -546 conjugated (Invitrogen) 1:1000. Confocal images were analysed using ImageJ.

Cardiac-specific mosaic overexpression of Wnt11:CFP

Wnt11:CFP fusion protein was cloned downstream of *cmlc2* promoter into the Tol2kit expression system using Gateway technology (Invitrogen). 10 μg/μl or 25 μg/μl of DNA was co-injected with 25 μg/μl capped Tol2 transposase mRNA into 1 cell stage embryos.

Drug treatment

Nifedipine 10μM (Sigma) or Bay K-8644 20μM (A.G. Scientific) was added to 30hpf old zebrafish embryos in egg water buffered with 5mM HEPES. Isolated zebrafish hearts were incubated in a mix of Thapsigargin 10μM (Sigma) and Caffeine 10mM (Sigma) in Tyrode's solution for 45 min prior to optical imaging.

Supplementary Material

Refer to Web version on PubMed Central for supplementary material.

Acknowledgments

We thank C.P. Heisenberg, L. Solnica-Krezel and J. Mably for the kind gifts of reagents. We thank R. Peterson and I. Drummond for critical comments on the manuscript. D.P. is supported by a fellowship from the HFSP. A.A.W. was supported by an NIH training award to the CVRC at MGH. C.A.M. is supported by the March of Dimes and the NIH. There are no competing interests. D.P. designed and performed the genetic, immunohistochemical and optical mapping experiments, A.A.W. devised techniques for optical voltage mapping and ratiometric Ca^{2+} imaging, developed analysis software, designed and performed these experiments, C.A.M. designed the experimental strategy. D.P., A.A.W. and C.A.M. analyzed the data and wrote the manuscript.

References

1. Costantini DL, et al. The homeodomain transcription factor Irx5 establishes the mouse cardiac ventricular repolarization gradient. Cell. 2005; 123:347–358. [PubMed: 16239150]
2. Yao L, McCaig CD, Zhao M. Electrical signals polarize neuronal organelles, direct neuron migration, and orient cell division. Hippocampus. 2009; 19:855–868. [PubMed: 19280605]
3. Adams DS, et al. Early, H+-V-ATPase-dependent proton flux is necessary for consistent left-right patterning of non-mammalian vertebrates. Development. 2006; 133:1657–1671. [PubMed: 16554361]
4. Zhao M, et al. Electrical signals control wound healing through phosphatidylinositol-3-OH kinase-gamma and PTEN. Nature. 2006; 442:457–460. [PubMed: 16871217]
5. Watanabe T, Delbridge LM, Bustamante JO, McDonald TF. Heterogeneity of the action potential in isolated rat ventricular myocytes and tissue. Circ Res. 1983; 52:280–290. [PubMed: 6825220]
6. Milan DJ, Giokas AC, Serluca FC, Peterson RT, MacRae CA. Notch1b and neuregulin are required for specification of central cardiac conduction tissue. Development. 2006; 133:1125–1132. [PubMed: 16481353]
7. Chi NC, et al. Genetic and physiologic dissection of the vertebrate cardiac conduction system. PLoS Biol. 2008; 6:e109. [PubMed: 18479184]
8. Hoyt RH, Cohen ML, Saffitz JE. Distribution and three-dimensional structure of intercellular junctions in canine myocardium. Circ Res. 1989; 64:563–574. [PubMed: 2645060]
9. Chung CY, Bien H, Entcheva E. The role of cardiac tissue alignment in modulating electrical function. J Cardiovasc Electrophysiol. 2007; 18:1323–1329. [PubMed: 17916158]

10. Auman HJ, et al. Functional modulation of cardiac form through regionally confined cell shape changes. PLoS Biol. 2007; 5:e53. [PubMed: 17311471]
11. Sehnert AJ, et al. Cardiac troponin T is essential in sarcomere assembly and cardiac contractility. Nat Genet. 2002; 31:106–110. [PubMed: 11967535]
12. Etard C, et al. The UCS factor Steif/Unc-45b interacts with the heat shock protein Hsp90a during myofibrillogenesis. Dev Biol. 2007; 308:133–143. [PubMed: 17586488]
13. Cohen ED, Tian Y, Morrisey EE. Wnt signaling: an essential regulator of cardiovascular differentiation, morphogenesis and progenitor self-renewal. Development. 2008; 135:789–798. [PubMed: 18263841]
14. Eisenberg CA, Eisenberg LM. WNT11 promotes cardiac tissue formation of early mesoderm. Dev Dyn. 1999; 216:45–58. [PubMed: 10474165]
15. Pandur P, Lasche M, Eisenberg LM, Kuhl M. Wnt-11 activation of a non-canonical Wnt signalling pathway is required for cardiogenesis. Nature. 2002; 418:636–641. [PubMed: 12167861]
16. Zhou W, et al. Modulation of morphogenesis by noncanonical Wnt signaling requires ATF/CREB family-mediated transcriptional activation of TGFbeta2. Nat Genet. 2007; 39:1225–1234. [PubMed: 17767158]
17. Flaherty MP, Dawn B. Noncanonical Wnt11 signaling and cardiomyogenic differentiation. Trends Cardiovasc Med. 2008; 18:260–268. [PubMed: 19232955]
18. Thisse C, Thisse B. High throughput expression analysis of ZF-models Consortium clones. ZFIN direct data submission. 2005http:/zfin.org
19. Robu ME, et al. p53 activation by knockdown technologies. PLoS Genet. 2007; 3:e78. [PubMed: 17530925]
20. Yao S, et al. Pnas4 is a novel regulator for convergence and extension during vertebrate gastrulation. FEBS Lett. 2008; 582:2325–2332. [PubMed: 18538138]
21. Heisenberg CP, et al. Silberblick/Wnt11 mediates convergent extension movements during zebrafish gastrulation. Nature. 2000; 405:76–81. [PubMed: 10811221]
22. Veeman MT, Axelrod JD, Moon RT. A second canon. Functions and mechanisms of beta-catenin-independent Wnt signaling. Dev Cell. 2003; 5:367–377. [PubMed: 12967557]
23. Jessen JR, et al. Zebrafish trilobite identifies new roles for Strabismus in gastrulation and neuronal movements. Nat Cell Biol. 2002; 4:610–615. [PubMed: 12105418]
24. Veeman MT, Slusarski DC, Kaykas A, Louie SH, Moon RT. Zebrafish prickle, a modulator of noncanonical Wnt/Fz signaling, regulates gastrulation movements. Curr Biol. 2003; 13:680–685. [PubMed: 12699626]
25. Slusarski DC, Corces VG, Moon RT. Interaction of Wnt and a Frizzled homologue triggers G-protein-linked phosphatidylinositol signalling. Nature. 1997; 390:410–413. [PubMed: 9389482]
26. Bers DM. Calcium cycling and signaling in cardiac myocytes. Annu Rev Physiol. 2008; 70:23–49. [PubMed: 17988210]
27. Stainier DY, et al. Mutations affecting the formation and function of the cardiovascular system in the zebrafish embryo. Development. 1996; 123:285–292. [PubMed: 9007248]
28. Witzel S, Zimyanin V, Carreira-Barbosa F, Tada M, Heisenberg CP. Wnt11 controls cell contact persistence by local accumulation of Frizzled 7 at the plasma membrane. J Cell Biol. 2006; 175:791–802. [PubMed: 17130287]
29. Rottbauer W, et al. Reptin and pontin antagonistically regulate heart growth in zebrafish embryos. Cell. 2002; 111:661–672. [PubMed: 12464178]
30. Angers S, Moon RT. Proximal events in Wnt signal transduction. Nat Rev Mol Cell Biol. 2009; 10:468–477. [PubMed: 19536106]

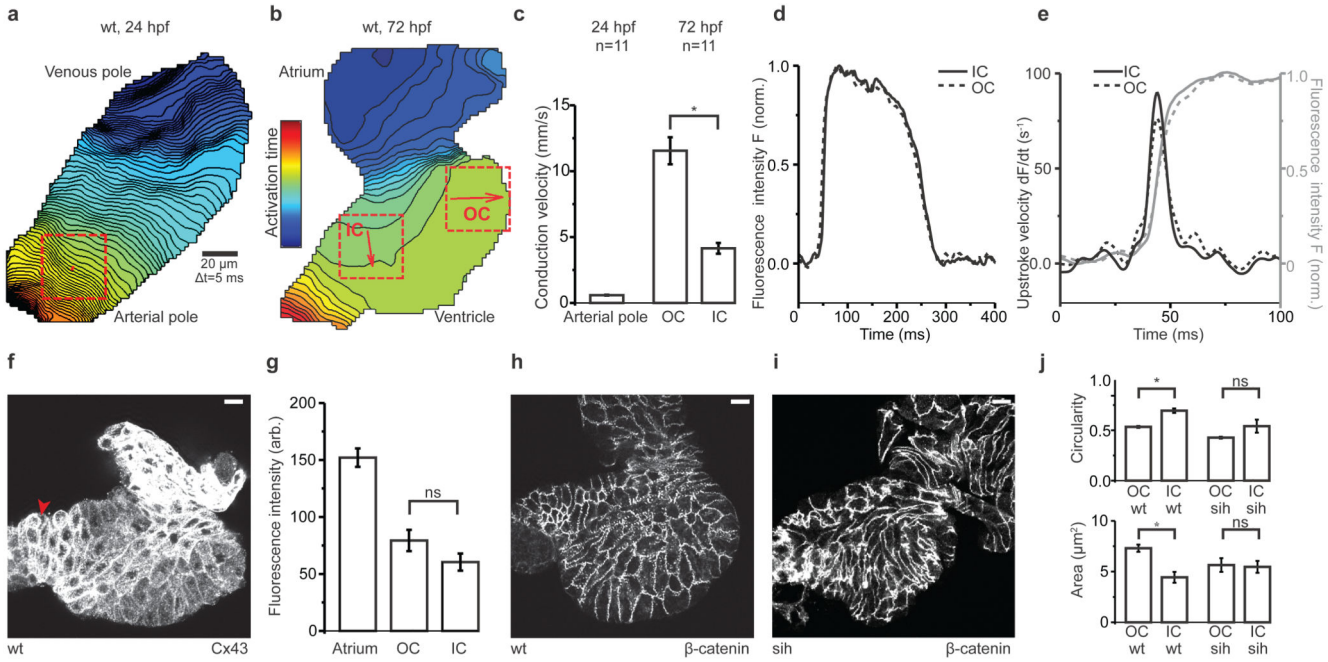

Figure 1. Formation of a myocardial electrical gradient in the developing zebrafish ventricle

a, **b**, Isochronal maps of wildtype hearts at 24hpf (**a**) and 72hpf (**b**). Each line represents the action potential wavefront position at 5 ms intervals. The colour code depicts the timing of electrical activation (blue areas activated before red areas). Squares indicate regions of interest (ROI) for conduction velocity estimation. The red arrows represent the average velocity vectors: an integral of the mean direction and speed of electrical impulse propagation, in the corresponding ROI. OC=outer curvature, IC=inner curvature.

c, Mean estimated conduction velocities from ROIs in **a** and **b**. Student's t-test, *p<0.05.

d, Averaged action potentials (n=5) from OC and IC ROIs at 72hpf.

e, Upstrokes (grey) and derived upstroke velocities (black) of action potentials in **d**.

f, Z projection of 2µm confocal section from a wild-type heart stained with anti-Cx43. The arrowhead points to outflow tract cardiomyocytes with slightly elevated Cx43 levels.

g, Average fluorescence intensities of respective ROIs from Cx43-stained hearts (n=10). Student's t-test, ns:p=0.13.

h, **i**, Z projection of 1µm confocal section from a wild-type heart (**h**) and *silent heart* (**i**) stained with anti-β-catenin.

j, Mean ventricular cardiomyocyte circularity index and cell area from wildtype (n=4) and *silent heart* embryos (n=4). Student's t-test, *p<0.05 (wt circularity), ns:p=0.13 (*sih* circularity), *p<0.05 (wt area), ns:p=0.85 (*sih* area).

f, **h**, **i**, 72hpf hearts, atrium at top. Scale bar = 10 µm. **c**, **g**, **j**. Error bars depict SEM.

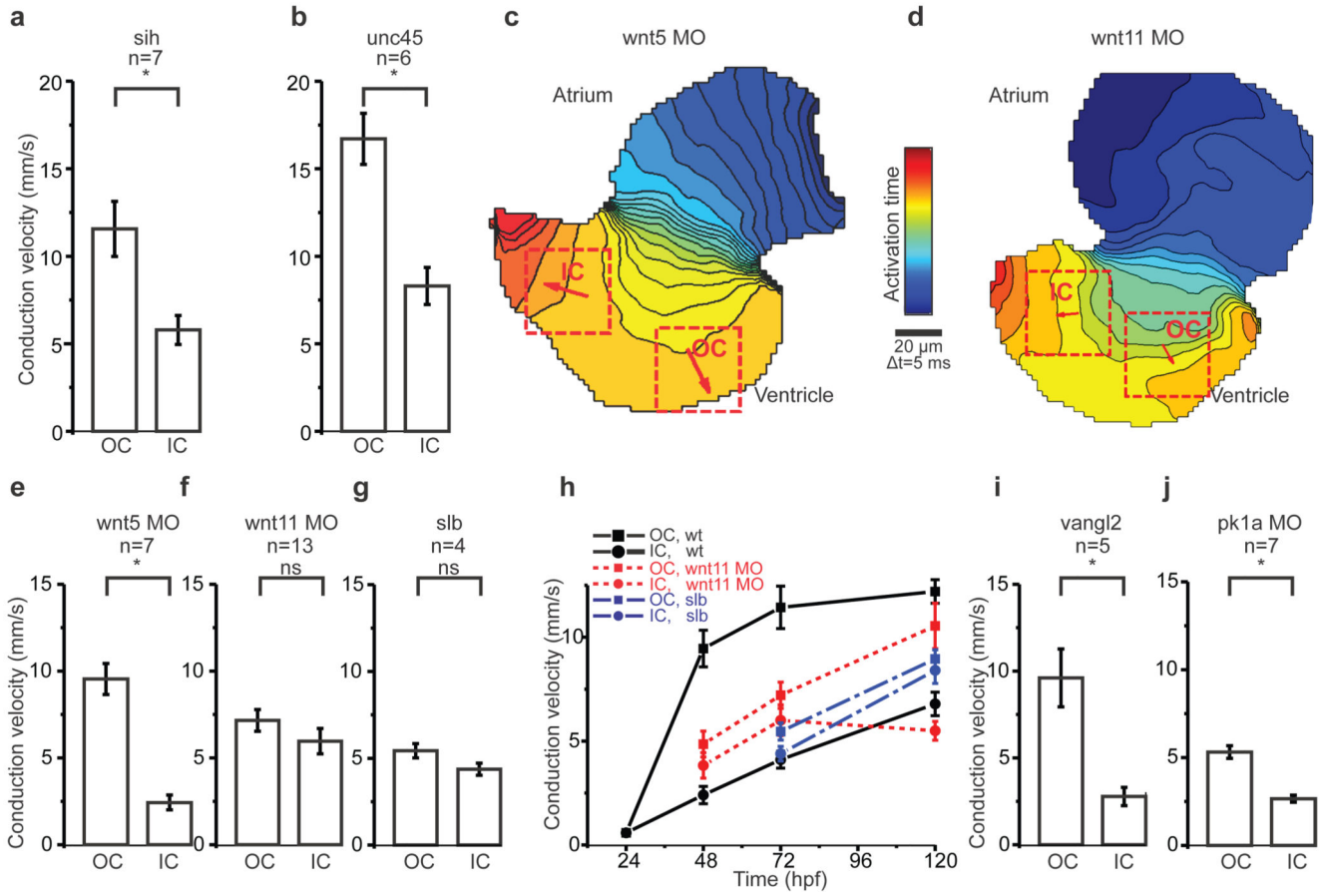

Figure 2. Loss of Wnt11 prevents myocardial electrical gradient formation

a, **b**, Mean estimated conduction velocities from *silent heart* (**a**), *p<0.05 and unc45 (**b**), *p<0.05.

c, **d**, Isochronal maps of hearts from Wnt5 (**c**) and Wnt11 (**d**) morphants. The colour code depicts the timing of electrical activation. Squares indicate ROIs for conduction velocity estimation. Arrows depict average velocity vectors in each ROI. OC=outer curvature, IC=inner curvature.

e, **f**, **g**, Mean estimated conduction velocities from Wnt5 (**e**), *p<0.05 and Wnt11 (**f**) morphants, p=0.22 and *silberblick* (**g**), p=0.10.

h, Time course of mean conduction velocities from 24hpf to 120hpf in the outer curvature (OC, squares) and inner curvature (IC, circles) from wildtype (in black), Wnt11 morphants (in red) and *silberblick* mutants (in blue).

i, **j**, Mean estimated conduction velocities from *vangl2* mutants (**i**), *p<0.05 and prickle1a morphants (**j**), *p<0.05.

Student's t-test was used to assess significance in each case. Error bars depict SEM. All experiments were performed at 72hpf.

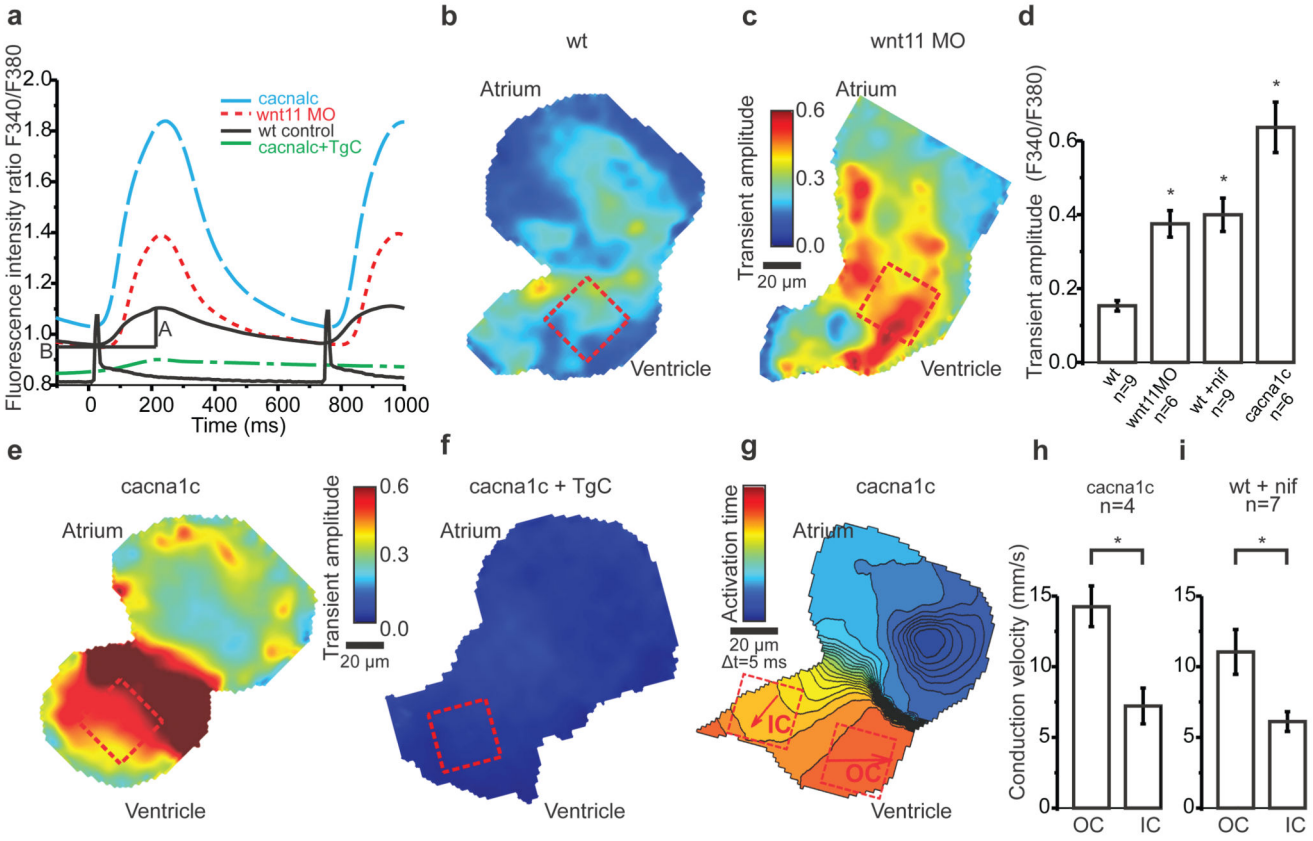

Figure 3. Wnt11 regulates Ca^{2+} transient amplitudes in cardiomyocytes

a, Averaged Ca^{2+} transients from ROIs in **b**, **c**, **e**, **f**. A = amplitude and B = baseline.

b, **c**, **e**, **f**, Colour maps of Ca^{2+} transient amplitudes from wildtype hearts (**b**), Wnt11 morphants (**c**), *cacna1c* (**e**) and *cacna1c*+thapsigargin+caffeine-treated embryos (**f**). Colour code depicts Ca^{2+} transient amplitudes in fluorescence ratio units (F340/F380). Squares indicate ROIs for measurements averaged in **a** and **d**.

d, Mean Ca^{2+} transient amplitudes. One-way ANOVA, *p<0.05 for comparisons with wildtype. Error bars depict SEM.

g, Isochronal map of *cacna1c* heart. The colour code depicts timing of activation. Squares indicate ROIs for conduction velocity estimation. Arrows display average velocity vector in each ROI. OC=outer curvature, IC=inner curvature.

h, **i**, Mean estimated conduction velocities of *cacna1c* (**h**) and nifedipine-treated (**i**) hearts. Student's t-test, *p<0.05. Error bars depict SEM.

All experiments were performed at 72hpf.

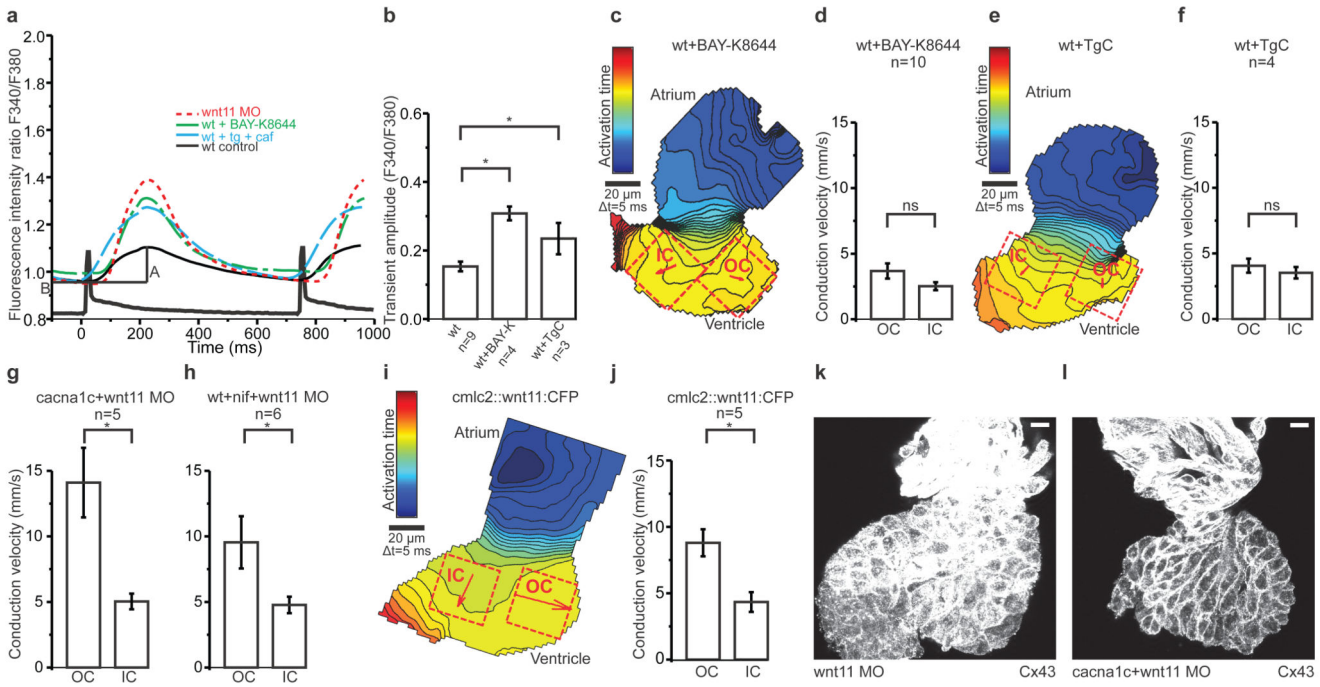

Figure 4. Wnt11 patterns electrical coupling through effects on transmembrane Ca^{2+} conductance

a, Averaged Ca^{2+} transients from ROIs in Figure 3 b, c and Supplementary Figure 5 c, d. A = amplitude and B = baseline.

b, Mean Ca^{2+} transient amplitudes. One-way ANOVA for comparisons with wildtype, *p<0.05.

c, **e**, **i**, Isochronal maps of Bay-K 8644- (**c**) and thapsigargin+caffeine- (**e**) –treated hearts and the heart of an embryo injected with 25 µg/µl of clmc2::wnt11:CFP (**i**). The colour code depicts the timing of activation. Squares indicate ROIs for conduction velocity estimation. Arrows display average velocity vectors. OC=outer curvature, IC=inner curvature.

d, **f**, **g**, **h**, **j**, Mean estimated conduction velocities from Bay-K 8644- (**d**), p=0.10, and thapsigargin+caffeine- (**f**), p=0.47, –treated hearts; hearts from *cacna1c* embryos injected with Wnt11MO (**g**), *p<0.05, hearts isolated from nifedipine-treated Wnt11 morphant embryos (**h**), *p<0.05, and cmlc2::wnt11:CFP injected embryos (**j**), *p<0.05. Student's t-test was used to assess significance in each case. Error bars depict SEM.

k, **l**, Z projection of 2µm confocal section from from Wnt11 morphant (**k**) and *cacna1c* mutant injected with Wnt11 MO (**l**), both stained with anti-Cx43. Scale bar = 10 µm. All experiments were performed at 72hpf.